# Effects of completeness and purity on cluster dark energy constraints

Michel Aguena* and Marcos Lima
*Departamento de Física Matemática, Instituto de Física, Universidade de São Paulo, CP 66318, CEP 05314-970 São Paulo, SP, Brazil*

(Received 21 November 2016; published 27 December 2018)

The statistical properties of galaxy clusters can only be used for cosmological purposes if observational effects related to cluster detection are accurately characterized. These effects include the selection function associated with cluster-finder algorithms and survey strategy. The importance of the selection becomes apparent when different cluster finders are applied to the same galaxy catalog, producing different cluster samples. We consider parametrized functional forms for the observable-mass relation, its scatter, as well as the completeness and purity of cluster samples, and study how prior knowledge on these function parameters affects dark energy constraints derived from cluster statistics. Under the assumption of a fiducial model for the selection function where the completeness and purity reach 50% at masses around $10^{13.5}\ M_\odot/h$, we find that self-calibration of selection parameters in current and upcoming cluster surveys is possible, while still allowing for competitive dark energy constraints. We consider a fiducial survey with specifications similar to those of the Dark Energy Survey with 5000 deg$^2$, maximum redshift of $z_{\rm max} \sim 1.0$ and threshold observed mass $M_{\rm th} \sim 10^{13.8}\ M_\odot/h$, such that the completeness and purity ∼60%–80% at masses around $M_{\rm th}$. Perfect knowledge of all selection parameters allows for constraining a constant dark energy equation of state to $\sigma(w) = 0.033$. Employing a joint fit including self-calibration of the effective selection degrades constraints to $\sigma(w) = 0.046$. External calibrations at the level of 1% in the parameters of the observable-mass relation and completeness/purity functions are necessary to improve the joint constraints to $\sigma(w) = 0.041$. Given the lack of knowledge of selection parameters, future experiments probing larger areas and greater depths may suffer from stronger relative degradations on dark energy constraints compared to current surveys.

DOI: 10.1103/PhysRevD.98.123529

## I. INTRODUCTION

The properties of dark matter halos have been characterized with increasing accuracy through dark matter $N$-body simulations of multiple cosmological models [1–7]. However, clusters of galaxies observed in surveys spanning different wavelengths carry a number of observational effects [8–15]. For the cosmological use of galaxy clusters, it is necessary to understand these effects in detail (e.g., by measuring them in simulations) and use this knowledge to parametrize the effects as appropriate functions of intrinsic cluster parameters (e.g., mass and redshift). An ideal self-consistent analysis must then constrain both cosmological parameters of interest as well as nuisance parameters related to astrophysical and observational effects, despite intrinsic degeneracies [8–10,16–23]. In this context, external calibrations of nuisance parameters may help to improve cosmology constraints.

Given a set of true halos and the matter tracers associated to them (e.g., optical galaxies), the first step is to characterize the performance of algorithms for cluster identification called cluster finders. Some of these methods—such as MaxBCG [24], FoF used in Ref. [25] and redMaPPer [26,27]—are based on the presence of red-sequence galaxies within clusters. They have the advantage of including this extra information, which is certainly valuable at low redshifts. However, they may suffer from limitations at higher redshifts. Meanwhile, there are cluster finders—such as WAZP [28], VT [29], and C4 [30]—that rely mostly on detecting spatial overdensities. These algorithms provide better detections at higher redshifts, although they typically depend more strongly on the quality of galaxy photometric redshifts.

Cluster finders may fail to identify a fraction of clusters related to dark matter halos, as well as detect false clusters with no association to halos. These two problems can be quantified by the so-called *completeness* and *purity* of the cluster sample [14,15,29], which typically reflect limitations of the cluster-finder algorithm, such as, e.g., artificial over-merging or fragmentation of clusters relative to their corresponding halos. Whereas the completeness and purity may depend on various factors—such as survey specifications, the quality of photometric redshifts (photo-$z$'s) and the observable-mass relation—they are mainly properties

*aguena@if.usp.br

 

of the cluster finder itself. We will often refer to the completeness and purity as describing the cluster selection function.

Next we must consider the *observable-mass* relation, typically characterized by a mean relation and a scatter [8,9,16,17]. For optical clusters the observable is the cluster richness, representing the number of cluster member galaxies. Richness may also refer to a subsample of member galaxies whose properties are more closely related to halo mass (e.g., richness can be based on red-sequence galaxies within a cluster [26,27], as opposed to all member galaxies). In simulations, clusters correctly matched to dark matter halos can be used to characterize the observable-mass relation [14,31–35]. However, it is important to point out that all of these calibrations are not enough to determine observable-mass and selection parameters at the percent level, even though they are still useful to help determine at least appropriate functional forms or loose priors for parameters, which are then self-calibrated in a full cosmological analysis. Observationally, optical clusters may be matched to detections in other wavelengths (e.g., millimeter or x-ray) from which observable-observable scaling relations can be estimated [36–38], and under the assumption of hydrostatic equilibrium, observable-mass relations may be derived. Alternatively, lensing masses may be available for a fraction of the optical clusters [39–45]. In conjunction, simulations and observational cross-matches allow for independent external calibrations of the observable-mass relation.

The scatter in the observable-mass relation may also be assessed from simulations and observations, and it can be tied to different sources [13]. An intrinsic scatter exists even for a perfect cluster finder (i.e., one with unit completeness and purity) and represents instances where a cluster of given richness has a range of masses due to intrinsic variability in the physical processes that relate these quantities, making them stochastic [31,32]. On the other hand, imperfections in the matching of clusters may artificially change this otherwise intrinsic scatter or lead to other observational issues [13]. We will also refer to the *effective* selection function, which is characterized by a combination of the actual selection function (completeness/purity) and the observable-mass relation.

There may be an interplay between the derived observable-mass relation and the sample selection function, as the characterizations of both depend on the matching process of clusters and halos (in simulations) and clusters and clusters (in multiwavelength observations). For instance, clusters catastrophically scattered in and out of a given richness bin may affect the sample completeness and purity, an effect which may be parametrized by altering the observable-mass distribution to include an extra Gaussian term [12]. Conversely, using only clusters and/or halos which are believed to have been correctly matched to define the observable-mass relation may produce a relation with unrealistically low scatter. Despite these issues, it is conceptually simpler to keep the definitions of the completeness and purity decoupled from the observable-mass relation, and we will follow this approach in this work by parametrizing these functions independently using functional forms characterized in simulations [46].

Finally, we must characterize errors in the cluster photometric redshifts (photo-$z$'s) [10]. We will again take the simpler approach of decoupling photo-$z$ errors from completeness and purity issues, as photo-$z$ errors are mainly tied to degeneracies in color-magnitude-redshift space and the efficiency of photo-$z$ algorithms [47–49]. The selection function of cluster finders that make direct use of photo-$z$'s [29,43] is clearly affected by the photo-$z$ quality, which may translate to additional sources of over-merging and fragmentation of clusters in the line of sight. However, for cluster galaxies we expect the photo-$z$ errors to be considerably smaller than for field galaxies. Therefore in this work we will neglect such effects, as our goal is to assess the direct impact of completeness and purity issues on cluster cosmology. Our analysis is conservative in this sense, since including the extra dependencies of the completeness and purity on observable-mass and photo-$z$ parameters would effectively decrease the number of nuisance parameters to constrain, potentially increasing the sensitivity of cluster observables.

In this paper we study how the inclusion of the cluster sample completeness and purity impacts the cosmological constraints derived from that sample. For a given parametrization of these functions, we also explore how prior knowledge on the selection can help constrain dark energy parameters in current and upcoming galaxy surveys. We start in Sec. II by discussing the characterization of the selection function via the sample completeness and purity. In Sec. III we discuss the formalism for predicting cluster counts and covariance, including selection effects. In Sec. IV we detail the Fisher matrix formalism to predict dark energy constraints and biases from cluster statistics, and in Sec. V we present the fiducial model, including selection parametrizations. In Sec. VI we present our main results, and in Sec. VII we discuss these results and conclude.

## II. COMPLETENESS AND PURITY

We define the *completeness* of a cluster catalog as the fraction of galaxy clusters *correctly* identified relative to the number of *true* dark matter halos. Likewise, the *purity* of the same catalog is defined as the fraction of galaxy clusters correctly identified relative to the *total* number of detected clusters. Clearly both concepts are important to characterize the cluster finder selection function, since nearly all algorithms lead to samples that are both incomplete and impure in certain ranges of masses and redshifts. A low completeness indicates an inefficiency of the cluster finder in detecting systems that it should have detected (or which a

perfect cluster finder detects), whereas a low purity indicates a high fraction of false positives in the sample, i.e., detections incorrectly made (and which a perfect cluster finder would not have made).

The completeness and purity of a cluster finder depend on the assumptions it makes and also on the observing conditions of a specific survey. For instance, a cluster finder which uses information from the galaxy red sequence—observed in most low-redshift clusters—has the possibility of outperforming a cluster finder that ignores this information. On the other hand, if the assumption of a red sequence is extrapolated into a domain in which it may not apply (e.g., at higher redshifts), such a cluster finder may produce samples that are either incomplete or impure. As a result, different performances may be observed when comparing different cluster finders applied to the same data set as well as the same cluster finder applied to different surveys.

From the above definitions of the completeness and purity, these quantities require matching clusters to dark matter halos. Strictly speaking, this can only be directly assessed in simulated catalogs, where information about the true underlying dark matter halos is fully available. However, cross-checks from real observations may also provide useful hints about the selection function of a given cluster finder. Here we will assume that simulations representative of the observing conditions are available for purposes of roughly estimating the cluster-finder selection function as well as the observable-mass relation. Clearly, simulations of this kind necessarily make certain assumptions that may not apply to real observed data. Nonetheless, they are useful to roughly calibrate cluster finders and estimates of their selection under these assumptions. When performing a cosmological analysis on real data, one would not fully trust simulation results, but they might inspire functional forms for parametrizing the cluster selection and observable-mass relation [31,32], whose parameter values can then be obtained from a self-consistent cosmological analysis of the cluster sample.

For pedagogical reasons, let us outline the process of using a simulated galaxy catalog and its associated dark matter halos for defining the cluster sample completeness, purity, and observable-mass relation. Given the list of true dark matter halos of mass $M$ and redshift $z$, and the catalog of galaxies populating these halos, one may run a cluster finder producing a list of clusters with certain observed properties (e.g., richness and photo-$z$'s for optical clusters). Since the considerations made here apply to detections not only of optical clusters but also for multiple wavelengths, we will often refer to the *observed mass* $M^{\rm obs}$ instead of the direct observable $\mathcal{O}$. Our fiducial survey will be similar to the Dark Energy Survey (DES), so we will typically refer to the richness as the observable, derived from optical cluster finders. However, all results also apply to cluster finders defined at other wavelengths with different mass proxies. Here $M^{\rm obs}$ is the mass inferred from the observable, being therefore equivalent to it, but in mass units. We will formally characterize individual clusters by their values of $M^{\rm obs}$ and photo-$z$, denoted $z^{\rm phot}$, and this notation applies even when we consider a specific observable such as richness. Given the number of halos $N_{\rm h}$ found and the number of clusters $N_{\rm c}$ detected, we may then consider the following steps towards characterizing the cluster-finder selection function and the observable-mass distribution:

(1) Rank the $N_{\rm h}$ halos by mass $M$ and the $N_{\rm c}$ clusters by richness $\mathcal{O}$.
(2) Perform a matching of halos and clusters, producing $N_{\rm mat}$ matches.
   (i) In general, the matching of halos and clusters can be done in two ways: by the fraction of coincident halo and cluster members, or by the spatial proximity of halo and cluster centers (either three-dimensional or angular).
   (ii) In cases where multiple matches may potentially occur (e.g., within a cluster radius one finds more than one halo center), the most massive halo or richest cluster may be selected among the possible candidates. This assures that, e.g., the most massive halo that is spatially close to the richest unmatched cluster will preferentially produce a match.
   (iii) A two-way matching can be applied to reassure a more stringent matching criterion. In this case the matching is made in both directions (halos are matched to clusters and vice versa) and only pairs that coincide in both directions are kept as true matches.
(3) Plot $\mathcal{O}$ versus $M$ for the matches to determine the observable-mass relation and its scatter. A cluster mass computed from this relation using the value of the observable $\mathcal{O}$ represents the cluster observed mass $M^{\rm obs}$.
(4) For each bin of halo mass $M$ and redshift $z$, compute the completeness $c(M,z)$ as

$$c(M,z) = \frac{N_{\rm mat}(M,z)}{N_{\rm h}(M,z)}. \tag{1}$$

(5) For each bin of cluster observed mass $M^{\rm obs}$ and photo-$z$ $z^{\rm phot}$, compute the purity $p(M^{\rm obs}, z^{\rm phot})$ as

$$p(M^{\rm obs}, z^{\rm phot}) = \frac{N_{\rm mat}(M^{\rm obs}, z^{\rm phot})}{N_{\rm c}(M^{\rm obs}, z^{\rm phot})}. \tag{2}$$

Clearly these definitions depend on the specific matching criterion imposed in the second step above (see further discussion on a related issue in Sec. III A). Notice that the ranking of halos and clusters in the very first step plays only a secondary role in the matching and is in fact dispensable. It enters only as an additional criterion to resolve potential multiple matches according to physical matching criteria

defined in the second step, either by membership overlap or spatial proximity.

We may also use these matches to estimate cluster $z^{\rm phot}$ errors, which depend both on the quality of galaxy photo-$z$'s and on the cluster-finder performance in assigning redshifts to clusters. In this work, we will assume that the effect of photo-$z$ errors is already encapsulated in the estimated completeness and purity and does not represent an extra source of cosmological degeneracies [10]. Obviously, such an assumption should be checked for each cluster finder, especially for those that rely heavily on galaxy photo-$z$ estimates.

In observed data, the estimation of the completeness and purity becomes intrinsically more complicated, as the mass of the clusters is not known and because no observed catalog can be taken as a truth table. Although the mass of the clusters can be estimated via observable-mass relations, the lack of a truth table makes the extraction of completeness and purity information from the data alone currently inviable. If reliable mock catalogs for a given survey are not available, the calibration of scaling relations is possible from lensing masses measured for a fraction of the detected clusters or from matching, e.g., optical clusters to detections at other wavelengths. Thus, we can obtain limited information about the observable-mass relation and its scatter. In the worst-case scenario, we could assume a generic selection function and fully self-calibrate its parameters (that is, to constrain the parameters along with the cosmology) from the observed cluster data alone. Fortunately, we expect reliable simulations, lensing masses, multiple external cross-calibrations, and spectroscopic follow-ups to be available for a self-consistent cosmological analysis of most current and future cluster surveys.

## III. OBSERVED CLUSTER PROPERTIES

### A. Cluster counts

We parametrize the theoretical dark matter halo mass function as

$$\frac{d\bar{n}(z,M)}{d\ln M}=\frac{\bar{\rho}_m}{M}\frac{d\ln\sigma^{-1}}{d\ln M}f(\sigma), \tag{3}$$

where $\sigma^2(M,z)$ is the variance of the linear density field in a spherical region of radius $R$ enclosing a mass $M=4\pi R^3\bar{\rho}_m/3$ at the present background matter density $\bar{\rho}_m$. We take $f(\sigma)$ from a fit to simulations by Tinker *et al.* [50], with parameter values appropriate for an overdensity $\Delta=200$ with respect to the background matter density. The predicted comoving number density $\bar{n}_\alpha$ of clusters in the observed-mass bin (indexed by $\alpha$) is obtained by integrating the mass function convolved with all observational effects mentioned previously as [8–10]

$$\bar{n}_\alpha(z)=\int_{M_\alpha^{\rm obs}}^{M_{\alpha+1}^{\rm obs}}d\ln M^{\rm obs}\int_0^\infty d\ln M\frac{d\bar{n}_{\rm obs}}{d\ln M}, \tag{4}$$

where the *observed* mass function

$$\frac{d\bar{n}_{\rm obs}}{d\ln M}=\frac{d\bar{n}(z,M)}{d\ln M}P(M^{\rm obs}|M)\frac{c(M,z)}{p(M^{\rm obs},z^{\rm phot})} \tag{5}$$

carries the effects of completeness, purity, and the observable-mass distribution $P(M^{\rm obs}|M)$, which is assumed to be Gaussian in $\ln M$. The number counts in the $i$th photo-$z$ bin are then obtained by integrating the comoving number density in comoving volume or redshift, including the photo-$z$ error distribution as [10]

$$\bar{m}_{\alpha,i}=\int_{z_i^{\rm phot}}^{z_{i+1}^{\rm phot}}dz^{\rm phot}\int_0^\infty dzP(z^{\rm phot}|z)\frac{r^2(z)}{H^2(z)}\bar{n}_\alpha(z), \tag{6}$$

where $H(z)$ is the Hubble parameter at redshift $z$ and $r(z)$ is the comoving angular diameter distance, identified here with the comoving radial distance since we only consider flat cosmologies. As mentioned previously, we will not consider the effect of photo-$z$ errors explicitly here. In the above description, this implies taking $P(z^{\rm phot}|z)$ to be a Dirac delta function, which then allows us to perform one of the redshift integrals trivially. In this case, we denote the *effective* cluster selection $f(M^{\rm obs}|M)$ as the combination

$$f(M^{\rm obs},z|M)=P(M^{\rm obs}|M)\frac{c(M,z)}{p(M^{\rm obs},z)}. \tag{7}$$

The separation of $f$ into these three components is mostly pedagogical, as the effective selection itself can be measured directly from simulations (with no reference to separate components). In fact, it is possible to consider completeness and purity effects (partially) as a propagation of projection effects into the otherwise intrinsic observable-mass relation $P(M^{\rm obs}|M)$, turning it into $f(M^{\rm obs}|M)$ [12]. Whereas simulations indicate that $P(M^{\rm obs}|M)$ can be parametrized as a log-Gaussian distribution [31–33,38,45,51] with observable-mass relations displaying low scatter [32], $f(M^{\rm obs}|M)$ would then have an extra log-Gaussian component, making the final distribution non-log-Gaussian [12].

Projection effects occur mainly as a result of photometric redshift errors, which cause cluster finders to fail in multiple ways. The simplest failure mode is when the cluster finder still detects individual clusters appropriately, but either includes field galaxies as cluster members or excludes true cluster members. In this case, projection effects conserve the total number of clusters and act merely as an extra source of scatter for richness estimates and could indeed be modeled as an extra log-Gaussian component for the observable-mass distribution. However, in more extreme cases of failure the cluster finder may

inappropriately fragment one cluster into two, merge two separate clusters along the line of sight into a single cluster, or simply fail to find a cluster due to a poor signal-to-noise ratio. These failure modes do not conserve the number of clusters and more strongly affect the measured cluster counts and variance. Our parametrization of selection in terms of the completeness and purity attempts to capture all of these possible cluster-finder failure modes.

As mentioned before, the observable-mass relation $P(M^{\rm obs}|M)$ has an intrinsic scatter due to the physical processes that correlate these quantities. This scatter can be studied and quantified in simulations and is well understood. However, there is an additional source of scatter related to the use of the observed mass and richness in $P(M^{\rm obs}|M)$. When calibrating $P(M^{\rm obs}|M)$, the uncertainties on the measurement of both the richness and the mass also have to be included [38]. For simplicity, we will not consider this extra observational effect.

However, contamination by projection effects is not the only issue that may affect the total selection. One simple effect (which, however, is likely always present) is a mismatch between the effective overdensity $\Delta_c$ used to define observed clusters and the overdensity $\Delta_h$ of the dark matter halos associated to them (either halos directly matched to clusters in simulations or halos whose mass function is used to predict the cluster abundance). For instance, if we use a halo mass function appropriate for $\Delta_h$ to predict the *cluster* abundance as described above, but our cluster finder detects clusters at an effective overdensity $\Delta_c \neq \Delta_h$, a mismatch of halo and cluster properties will follow if not accounted for explicitly. Notice that these effects may happen even for a perfect cluster finder, and because they are associated to the cluster detection itself, they cannot be corrected after detection by simply redefining cluster masses with a more appropriate overdensity or even a new observable. For clusters detected using signal-to-noise ratios or fixed apertures, which do not correspond to a fixed halo overdensity, it may be even trickier to interpret comparisons of cluster and halo properties.

From the considerations above, it is clear that the completeness and purity depend on specific assumptions underlying cluster-finder algorithms. In this work we will parametrize the selection via separate functions for the sample completeness and purity as described in Sec. V.

### B. Cluster covariance

The local number counts $m_{\alpha,i}(\mathbf{x})$ of clusters at position $\mathbf{x}$ fluctuate spatially around the mean predicted values $\bar{m}_{\alpha,i}$, following the matter density contrast $\delta(\mathbf{x})$ as

$$m_{\alpha,i}(\mathbf{x}) = \bar{m}_{\alpha,i}[1 + b_\alpha(z)\delta(\mathbf{x})], \tag{8}$$

where $b_\alpha(z)$ is the average cluster bias defined as

$$b_\alpha(z) = \frac{1}{\bar{n}_\alpha(z)} \int_0^\infty d\ln M \frac{d\bar{n}_\alpha}{d\ln M} b(M,z). \tag{9}$$

Notice that $b_\alpha(z)$ is consistently predicted from the number density in Eq. (4), and therefore carries the observable-mass and selection effects. Here $b(M,z)$ is the halo bias for which we will take a fit to simulations by Tinker *et al.* [52] as

$$b(M,z) = 1 - A\frac{\nu^a}{\nu^a + \delta_c^a} + B\nu^b + C\nu^c, \tag{10}$$

where $\nu(M,z) = \delta_c/\sigma(M,z)$, $\delta_c = 1.686$, and we fix values for the parameters $A$, $B$, $C$, $a$, $b$, $c$ that are appropriate for the same overdensity $\Delta = 200$ used in the abundance predictions.

The cluster counts have a sample covariance $S_{ij}^{\alpha\beta}$ due to the large-scale structure of the Universe given by [9,53]

$$\begin{aligned} S_{ij}^{\alpha\beta} &= \langle (m_{\alpha,i} - \bar{m}_{\alpha,i})(m_{\beta,j} - \bar{m}_{\beta,j})\rangle \\ &= \bar{m}_{\alpha,i} b_{\alpha,i} \bar{m}_{\beta,j} b_{\beta,j} \int \frac{d^3k}{(2\pi)^3} P(k) W_i^*(\mathbf{k}) W_j(\mathbf{k}), \end{aligned} \tag{11}$$

where $W_i(\mathbf{k})$ is the Fourier transform of the volume window function in bin $i$ and we set $b_{\alpha,i} \approx b_\alpha(z_i)$ at the bin centroid $z_i$, which is valid for sufficiently small redshift bins.

Here we will take a window to be a cylinder with a small angular radius ($\theta_s \lesssim 10$ deg) and height $\delta r_i$, in which case $W_i(\mathbf{k})$ is given by [10,54]

$$W_i(\mathbf{k}) = 2\exp(ik_\parallel r_i) j_0\left(\frac{k_\parallel \delta r_i}{2}\right) \frac{J_1(k_\perp \theta_s r_i)}{k_\perp \theta_s r_i}, \tag{12}$$

where $\mathbf{k} = (k_\parallel, \mathbf{k}_\perp)$. The counts are also subject to Poisson variance or shot noise given by

$$M_{ij}^{\alpha\beta} = \delta_{\alpha\beta}\delta_{ij}\bar{m}_{\alpha,i}, \tag{13}$$

such that the total covariance $C_{ij}^{\alpha\beta}$ is the sum of the sample covariance and Poisson variance,

$$C_{ij}^{\alpha\beta} = S_{ij}^{\alpha\beta} + M_{ij}^{\alpha\beta}. \tag{14}$$

## IV. FISHER MATRIX

We use the Fisher matrix formalism to study the effects of parametrizing the cluster selection function, given the predictions of cluster counts and covariance described in the previous section. We split the counts into redshift, mass, and angular cells. For convenience of notation, we let the index $i$ denote binning in photo-$z$, observed mass, and angular pixel, and arrange the counts into a single vector $\bar{\boldsymbol{m}}$. Similarly, we arrange the sample covariance, Poisson

variance, and total covariance of $\bar{\boldsymbol{m}}$ into matrices $\boldsymbol{S}$, $\boldsymbol{M}$, and $\boldsymbol{C} = \boldsymbol{S} + \boldsymbol{M}$.

Given a set of parameters $\theta_\alpha$, the Fisher matrix quantifies the information in both the cluster counts and cluster covariance as [9,10]

$$F_{\alpha\beta} = \bar{\boldsymbol{m}}_{,\alpha}\boldsymbol{C}^{-1}\bar{\boldsymbol{m}}_{,\beta}{}^{T} + \frac{1}{2}\mathrm{Tr}[\boldsymbol{C}^{-1}\boldsymbol{S}_{,\alpha}\boldsymbol{C}^{-1}\boldsymbol{S}_{,\beta}], \quad (15)$$

where the first term contains information on the counts and the second term contains information on the covariance of these counts. The clustering properties of galaxy clusters—encoded in their covariance—bring extra information to the cluster counts, which helps with the self-calibration (constraining nuisance parameters along with the cosmology) of the observable-mass distribution [9,10,17,18,51] and (as we shall see) the cluster selection function. The inverse Fisher matrix approximates the covariance matrix of the parameters $C_{\alpha\beta} \approx [F^{-1}]_{\alpha\beta}$. The marginalized error on a single parameter $\theta_\alpha$ is $\sigma(\theta_\alpha) = [F^{-1}]^{1/2}_{\alpha\alpha}$. In case we have *prior* information on parameter $\theta_\alpha$ at the level of $\sigma_p(\theta_\alpha)$, we add to the Fisher matrix a diagonal contribution of $\sigma_p^{-2}(\theta_\alpha)\delta_{\alpha\beta}$ before inversion.

Finally, variations of the number counts of $\Delta\bar{\boldsymbol{m}}$ and of the sample covariance of $\Delta\boldsymbol{S}$, relative to their values in the fiducial model, induce a systematic error or bias $b(\theta_\alpha) = \delta\theta_\alpha$ on a derived parameter $\theta_\alpha$, given by [12,55]

$$b(\theta_\alpha) = F^{-1}_{\alpha\beta}\left\{\bar{\boldsymbol{m}}_{,\beta}\boldsymbol{C}^{-1}\Delta\bar{\boldsymbol{m}} + \frac{1}{2}\mathrm{Tr}[\boldsymbol{C}^{-1}\boldsymbol{S}_{,\beta}\boldsymbol{C}^{-1}\Delta\boldsymbol{S}]\right\}. \quad (16)$$

This equation can be used to assess the bias on inferred cosmological parameters when neglecting the inclusion of selection function parameters, given that the true counts in the fiducial model require these additional parameters.

## V. FIDUCIAL MODEL

We choose a fiducial cosmology from a flat $w$CDM model with best-fit parameters consistent with the results from Planck [56] as $h^2\Omega_{\rm m} = 0.14$, $h^2\Omega_b = 0.022$, $w = -1$, $A_s = 2.13 \times 10^{-9}$ (corresponding to $\sigma_8 = 0.83$), $n_s = 0.96$, and $\tau = 0.089$. We also set priors of 1% on all parameters, except for $h^2\Omega_{\rm m}$ and $w$, which will vary freely as we wish to study the potential for galaxy clusters to constrain dark energy in the presence of cluster selection parameters.

We assume a survey area of 5000 deg$^2$, similar to that planned for the final observations of DES [57]. We consider the counts and covariance within 500 cells of 10 deg$^2$ each. To reflect expectations and limitations of cluster finders in current optical surveys, we restrict the analysis to nine redshift bins of $\Delta z = 0.1$ from $z = 0.1$ to $z_{\rm max} = 1.0$. We also include seven bins of observed mass of $\Delta\log[M^{\rm obs}/(M_\odot h^{-1})] = 0.2$ from a threshold mass of $M^{\rm obs}_{\rm th} = 10^{13.8}\ M_\odot/h$, where the last bin was reshaped to $\log[M^{\rm obs}/(M_\odot h^{-1})] = [15.0:17.0]$ to include all high-mass clusters. This binning choice leaves us with 63 bins of count measurements, which we expect to be sufficient to provide information on the observed mass and redshift evolution of the selection function and the observable-mass relation. The completeness and purity mostly shift each bin individually (although to consider the full effect of the completeness within an observed mass bin it is necessary to integrate over all masses; see Fig. 1). The scatter on the observable-mass relation spreads a portion of the clusters across different mass bins, and the mass bias systematically shifts clusters to higher (or lower) observed mass bins. This approach also allows us to test the cluster-constraining power when considering different minimum masses, by simply adding (or removing) mass bins.

The observable-mass $P(M^{\rm obs}|M)$ distribution will be assumed to be Gaussian in $\ln M$ with a scatter $\sigma_{\ln M}$ and bias $\ln M_{\rm bias}$,

$$P(M^{\rm obs}|M) = \frac{1}{\sqrt{2\pi\sigma^2_{\ln M}}}\exp\left[-\frac{\chi^2(M^{\rm obs})}{2}\right], \quad (17)$$

where

$$\chi(M^{\rm obs}) = \frac{\ln M^{\rm obs} - \ln M - \ln M_{\rm bias}}{\sigma_{\ln M}}. \quad (18)$$

We parametrize the evolution of the mass bias with redshift as [9]

$$\ln M_{\rm bias}(z) = A_b + n_b\ln(1+z), \quad (19)$$

where the fiducial values are $A_b = n_b = 0$. Since we expect the mass scatter in the relation to increase for high redshifts and low masses, we take

$$\frac{\sigma^2_{\ln M}(z,M)}{0.2^2} = 1 + B_0 + B_z(1+z) + B_M\left(\frac{\ln M_s}{\ln M}\right), \quad (20)$$

with the fiducial values of $B_0 = B_z = B_M = 0$ and we fix the pivot mass $M_s = 10^{14.2}\ M_\odot/h$.

As clusters of high mass stand out in observations, we expect less ambiguity in detecting them. Therefore, the completeness and purity should approach unity at high enough values of $M$ and $M^{\rm obs}$. Similarly, for low masses the number of clusters increases and we expect the confusion to be larger, so the completeness and purity decrease. We set a functional form for both the completeness and purity that interpolates between these two limits of high and low masses as

$$c(M,z) = \frac{[M/M_c(z)]^{n_c}}{[M/M_c(z)]^{n_c} + 1}, \quad (21)$$

$$p(M^{\rm obs}, z^{\rm phot}) = \frac{[M^{\rm obs}/M_p^{\rm obs}(z)]^{n_p}}{[M^{\rm obs}/M_p^{\rm obs}(z)]^{n_p}+1}, \quad (22)$$

where $M_c(z)$ and $M_p(z)$ are parametrized functions and we take the exponents $n_c$ and $n_p$ to be constants. This functional form was characterized and shown to describe well the completeness and purity in simulations [46]. We consider two different cases, as shown in Table I: case (1) uses $n_c = 3$ and $n_p = 1$, and therefore the ratio $c/p$ goes to zero in the limit of low $M$ and $M^{\rm obs}$; case (2) uses $n_c = 1$ and $n_p = 3$, and therefore the ratio $c/p$ goes to infinity in the limit of low $M$ and $M^{\rm obs}$. These two cases should bracket a reasonable range of possible parametrizations for the selection and their dependence on mass and redshift. For the mass scales $M_c$ and $M_p^{\rm obs}$, which control the transitions in the completeness and purity function, we use linear relations,

$$\log M_c(z) = \log \tilde{M}_c + c_0 + c_1(1+z), \quad (23)$$

$$\log M_p^{\rm obs}(z) = \log \tilde{M}_p^{\rm obs} + p_0 + p_1(1+z), \quad (24)$$

with fiducial values of $c_0 = p_0 = c_1 = p_1 = 0$. Here $\tilde{M}_c$ and $\tilde{M}_p^{\rm obs}$ are arbitrary pivot masses where the completeness and purity decrease to 50% in the fiducial model. For illustrative purposes we fix them to $\tilde{M}_c = 10^{13.6}\ M_\odot/h$ and $\tilde{M}_p^{\rm obs} = 10^{13.5}\ M_\odot/h$, which results in a completeness $\approx(80\%, 61\%)$ and purity $\approx(67\%, 89\%)$ around the threshold mass for cases (1,2).

For reference, we consider an additional case of perfect cluster detection, i.e., completeness and purity equal to unity for all masses and redshifts. We will denote this as case (0) and will consider the bias induced on dark energy parameters when case (0) is assumed whereas the true model is either case (1) or (2). We will also consider the dark energy constraints derived within cases (1) and (2) and the impact of prior knowledge on nuisance parameters describing the observable-mass relation and cluster selection.

The functional forms proposed for the completeness and purity are shown in the left panel of Fig. 1. While the purity is a function of the observed mass of clusters, the completeness depends on the true mass of the dark matter halos. Therefore for a given value of observed mass, the effective completeness results from the contribution of a range of true masses determined by the scatter in the observable-mass relation. This feature is illustrated in the left panel of Fig. 1, where the vertical red line indicates the fiducial observed mass threshold $M_{\rm th}^{\rm obs} = 10^{13.8}\ M_\odot h^{-1}$, and the red shaded regions delineate the scatter at the 1, 2, and $3\sigma_{\ln M}$ levels for the effective selection.

The right panel of Fig. 1 shows the ratio of the completeness and purity $(c/p)$, which affects the effective cluster selection in Eq. (7). For each of the cases (1) and (2), the ratio $c/p$ has limits indicated in Table I. In both cases, the ratio $c/p \to 1$ in the limit of high masses, since both $c$ and $p$ approach unity in this limit. For case (1) the ratio $c/p \to 0$ at lower masses; however, in the mass range investigated ($\geq 10^{13.8}\ M_\odot h^{-1}$), the ratio $c/p > 1$, resulting in more detected clusters than case (0). An opposite effect

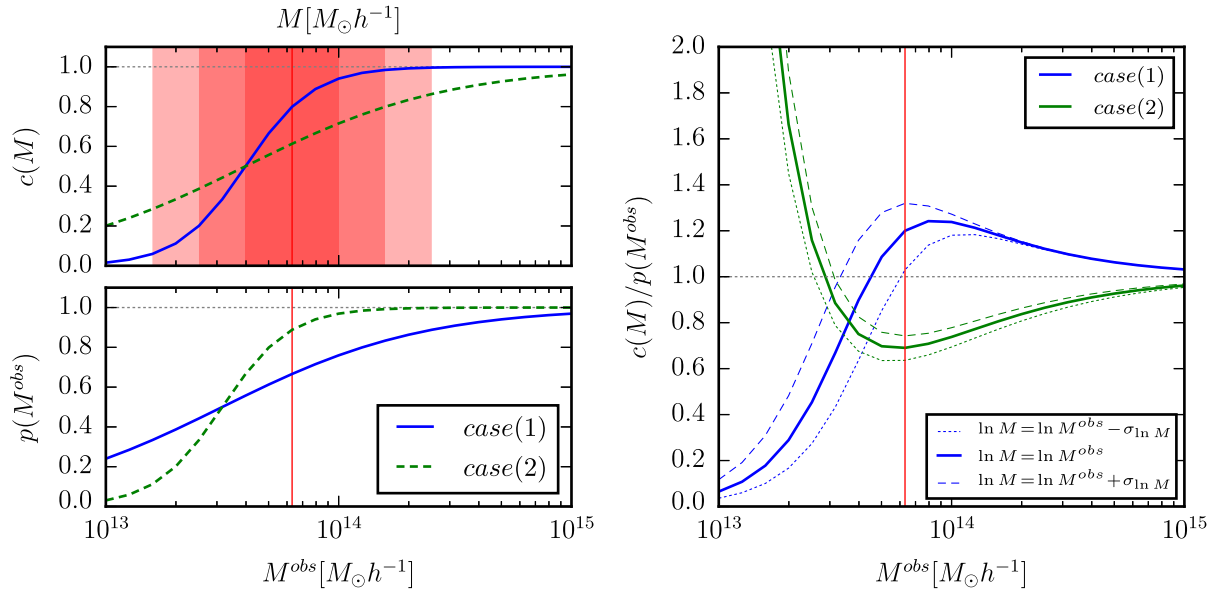


FIG. 1. Completeness and purity as a function of mass for cases (1) and (2) at $z = 0$. The red vertical line denotes the threshold mass $M_{\rm th}^{\rm obs} = 10^{13.8}\ M_\odot/h$ assumed in the fiducial model. Left: Both functions are shown separately and the red shaded regions display the mass spread around this threshold at 1, 2, and $3\sigma_{\ln M}$. Right: Ratio of completeness and purity [see Eq. (7)] as a function of mass. As a result, case (1) produces an increase in cluster counts for higher masses and a decrease at lower masses, while case (2) induces the opposite behavior.

TABLE I. Cases considered for completeness and purity parameter values.

| Case | Completeness | Purity | $c/p$ (as $M \to 0$) |
|---|---|---|---|
| 0 | $c = 1$ | $p = 1$ | 1 |
| 1 | $n_c = 3$ | $n_p = 1$ | 0 |
| 2 | $n_c = 1$ | $n_p = 3$ | $\infty$ |

occurs for case (2), resulting in fewer cluster detections. Although the region of very low masses ($M^{\rm obs} \sim 10^{13}\ M_\odot h^{-1}$) is not the focus of this work, it is interesting to analyze what happens to the ratio $c/p$ in this limit. For case (1), the completeness decreases faster than the purity, meaning that the capability of the cluster finder to detect objects goes to zero. The other case, where $c/p$ becomes large at low masses, happens when the purity decreases faster than the completeness. This may happen, for instance, as the cluster finder attempts to detect clusters whose BCG has a magnitude close to the survey limiting magnitude, particularly at low masses and high redshifts. As the cluster finder struggles with the detection, the number of false positives may become larger than the number of missed clusters.

Notice that by using multiple observables we attempt to self-calibrate various nuisance parameters describing the observable-mass relation and the selection effects. In reality, this will only be effective if the parametrizations used are indeed correct.

## VI. RESULTS

Before studying the impact of selection parameters on dark energy constraints, for illustrative purposes we first look at the effect on cluster abundance and clustering of each cosmological and nuisance parameter. Figure 2 shows the effects of cosmology and selection on the number counts (top) and the diagonal of the sample covariance (bottom) as a function of redshift (left) and mass (right), with selection parameters from case (1). The left panels (where different redshift bins are displayed) were computed in the mass bin $M^{\rm obs}_{\rm th} = [13.8\!:\!14.0]$, and the right panels were computed in the redshift bin $z = [0.6, 0.7]$, as those are the bins with the largest number of objects, and that thus have a more significant effect on the constraints. We note that the actual constraining results make use of all mass and redshift bins and the nondiagonal terms of the sample covariance.

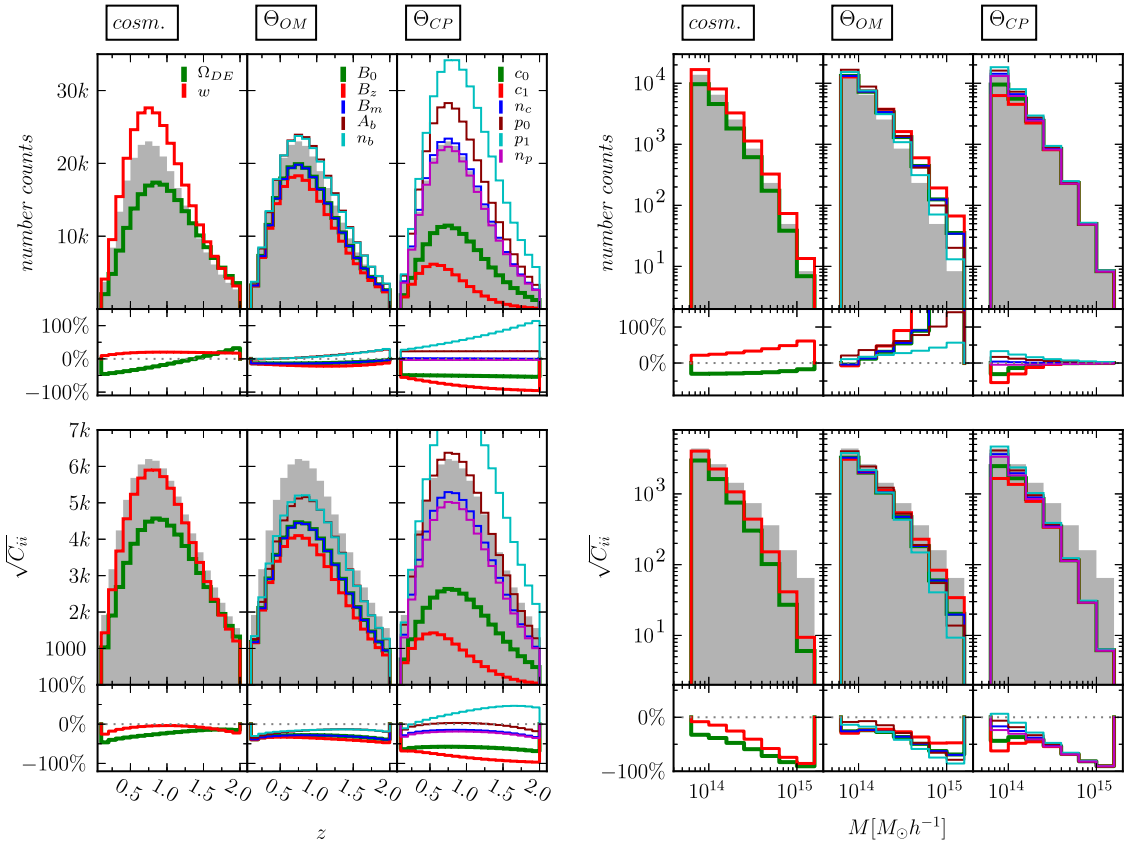


FIG. 2. Variation of the cluster number counts (top) and sample variance (bottom) as a function of redshift (left) and mass (right) for changes in the dark energy parameters, observable-mass relation, completeness, and purity, considering case (1). The left panels were computed for the mass bin $M^{\rm obs}_{\rm th} = [13.8\!:\!14.0]$ and the right panels for the redshift bin $z = [0.6, 0.7]$. The gray shaded region is the fiducial case, and the colored lines indicate a variation of $+0.2$ in each parameter.

We compute counts for the fiducial model (gray shaded region) and for positive variations of 0.2 in each parameter considered.

To evaluate some of the effects the parameters considered have on the constraints, let us explore the changes in the number counts as a function of redshift (top left panel of Fig. 2). We assume a flat universe, so an increase in $\Omega_{\rm DE}$ results in a decrease in $\Omega_m$, and the overall abundance of clusters is reduced. Increasing $w$ causes the dark energy behavior to be closer to that of nonrelativistic matter, also resulting in an increase in cluster counts.

From the definition of the mass bias $M_{\rm bias}$ in Eq. (18), increasing its value results in a lower effective mass threshold, therefore increasing the counts of clusters. The same is true for the mass scatter [9], though with a lower sensitivity compared to the mass bias.

Increasing the completeness parameters $c_0$ and $c_1$ increases the mass scale $M_c$ in which the completeness becomes 50%, lowering the values of the completeness across all masses and reducing the counts of detected clusters. An increase of $n_c$ makes the drop in the completeness at $M < M_c$ sharper, resulting in a slight increase of the completeness for $M > M_c$ and a decrease for $M < M_c$. Since the mass threshold adopted ($M_{\rm th}^{\rm obs} = 10^{13.8}\ M_\odot h^{-1}$) is higher than the fiducial value of $M_c$ ($10^{13.5}\ M_\odot h^{-1}$), increasing $n_c$ produces a slight increase in the counts.

Finally, given our effective cluster selection from Eq. (7), purity has an inverse effect compared to the completeness for the counts. In fact, since the completeness and purity have the same functional form, changes in each purity parameter cause opposite effects in counts compared to changes in the corresponding completeness parameter.

These results indicate how parameters are (anti)correlated, i.e., how changes in one parameter can compensate for changes in other parameters. The effects on the cluster counts described above, however, occur when all other parameters are fixed at their fiducial value. When marginalizing over parameters, the resulting correlations may change.

### A. Selecting cases

The first issue we consider is whether it is worth including completeness and purity parameters in the cluster analysis for purposes of constraining dark energy. Including extra nuisance parameters (related to the observational effects) increases the accuracy, but decreases the precision of cosmological constraints. When completeness and purity effects are ignored, i.e., when case (0) is assumed despite imperfect selection, the resulting cosmological parameters $\theta_\alpha$ constrained have a bias $b(\theta_\alpha)$ [Eq. (16)]. The assumption of perfect detection can still provide reliable cosmological parameter constraints as long as the bias is smaller than the parameter constraints,

$$b(\theta_\alpha) \lesssim \gamma\sigma(\theta_\alpha) = \gamma(F^{-1})^{1/2}_{\alpha\alpha}, \tag{25}$$

where $\gamma = 1, 2, 3$ indicate biased predictions at the 68, 95, and 99% confidence levels. Here $\Delta\bar{\boldsymbol{m}}$ and $\Delta\boldsymbol{S}$ in Eq. (16) are the differences in the counts and sample covariance between predictions in case (0) and cases (1) and (2).

Figure 3 shows the bias induced on the dark energy parameters $(\Omega_{\rm DE}, w)$ as a function of the observed mass threshold used $M_{\rm th}^{\rm obs}$ if we assume case (0), when in reality counts are described by cases (1) (solid line) and (2) (dashed line). Also shown are the 1, 2, and $3\sigma$ confidence levels on $(\Omega_{\rm DE}, w)$ in case (0) (blue shaded regions). This observed mass threshold we consider does not imply that only a single bin of mass is being used, but that mass bins of $\Delta\log[M^{\rm obs}/(M_\odot h^{-1})] = 0.2$ down to this threshold are being used. Therefore, $\log[M_{\rm th}^{\rm obs}/(M_\odot h^{-1})] = 13.8$ results in seven observable mass bins, while $\log[M_{\rm th}^{\rm obs}/(M_\odot h^{-1})] = 14.2$ considers only five observable mass bins. The bias on $\Omega_{\rm DE}$ has surpassed the $1\sigma$ constraints for thresholds $\log[M_{\rm th}^{\rm obs}/(M_\odot h^{-1})] \leq 14.2$ in both cases (1) and (2). In fact, the bias is larger than $2\sigma$ for case (1) and $3\sigma$ for case (2) around the fiducial threshold mass $\log[M_{\rm th}^{\rm obs}/(M_\odot h^{-1})] = 13.8$. The bias on $w$ is around $1\sigma$ at $\log[M_{\rm th}^{\rm obs}/(M_\odot h^{-1})] = 13.8$, indicating that this parameter is less sensitive to the selection effects. However, $w$ is less well constrained than $\Omega_{\rm DE}$ so a bias comparable to $1\sigma$

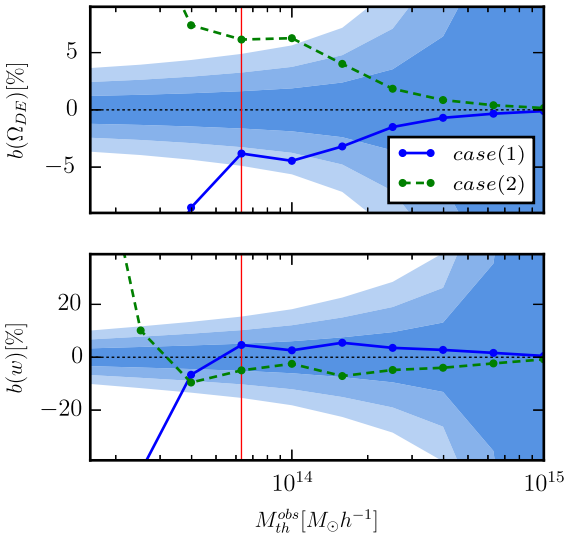


FIG. 3. Comparison between i) the 1, 2, and $3\sigma$ constraints (blue shaded regions) on the dark energy parameters $\theta_{\rm DE} = (\Omega_{\rm DE}, w)$ for case (0) of perfect cluster selection and ii) the percent bias $b(\theta_{\rm DE})$ (lines) on dark energy caused by ignoring completeness and purity effects as given by cases (1) and 2) (solid, dashed). As the bias becomes comparable to $1\sigma$ constraints $b(\theta_\alpha) \approx \sqrt{F^{-1}_{\alpha\alpha}}$, the assumption of perfect detection results in significantly incorrect best-fit predictions. For the considered threshold mass $\log[M_{\rm th}^{\rm obs}/(M_\odot h^{-1})] = 13.8$ (vertical red line), the bias $b(\Omega_{\rm DE})$ is larger than the corresponding $2\sigma$ constraint for both cases (1) and (2), whereas $b(w)$ is comparable with the $1\sigma$ constraint.

constraints may be even more significant when constraining models of dark energy.

Notice that the bias behavior as a function of $M_{\rm th}^{\rm obs}$ is not monotonic. This occurs mainly due to the fact that the ratio $c/p$ of the completeness and purity is also not monotonic, as seen in the right panel of Fig. 1. For very large thresholds, $c/p$ indeed approaches unity [as in case (0)] and the bias is small. For masses around the fiducial threshold, the bias is caused mainly by the upper/lower bump in $c/p$ for case (1)/(2). For lower masses, the bias becomes much larger and is dominated by the rapid change in $c/p$ for both cases (1) and (2).

Given that the minimum mass threshold that still allows for somewhat reliable dark energy constraints under case (0) is located at $14.2 < \log[M_{\rm th}^{\rm obs}/(M_\odot h^{-1})] < 14.4$, we now investigate for what mass thresholds the constraints under cases (1) and (2) become better than those from case (0) under $\log[M_{\rm th}^{\rm obs}/(M_\odot h^{-1})] = 14.2$ as a conservative comparison. As we go to lower threshold masses and need to fully model the selection with a larger number of nuisance parameters (describing the completeness and purity), we also considerably increase the number of clusters probed, which provides more cosmological information.

The left panel of Fig. 4 shows $1\sigma$ constraints for cases (0), (1), and (2) as a function of the observed mass threshold $M_{\rm th}^{\rm obs}$. The dotted lines mark the mass threshold $\log[M_{\rm th}^{\rm obs}/(M_\odot h^{-1})] = 14.2$ and the corresponding constraints for case (0). As we decrease the threshold mass, the constraints for cases (1) and (2) improve. At the fiducial threshold $\log[M_{\rm th}^{\rm obs}/(M_\odot h^{-1})] = 13.8$, the marginalized constraints of $\Omega_{\rm DE}$ and $w$ for both cases (1) and (2) are lower than those from case (0) with threshold $\log[M_{\rm th}^{\rm obs}/(M_\odot h^{-1})] = 14.2$.

The right panel of Fig. 4 shows the joint dark energy constraints for multiple cases at different thresholds. The solid and dashed lines correspond to cases (1) and (2) with the fiducial threshold, respectively, whereas the blue shaded region corresponds to case (0) and the higher threshold, for which this case is marginally reliable. We see that a fiducial threshold $\log[M_{\rm th}^{\rm obs}/(M_\odot h^{-1})] = 13.8$ is enough to significantly improve the dark energy constraints relative to case (0), despite the increase in the number of nuisance parameters from the selection function.

It is interesting to notice that, as we consider even lower threshold masses than the fiducial one assumed here, we continue to improve the dark energy constraints. However, that requires us to trust that the selection can still be well described by the parametrized functional forms assumed here down to those lower masses. That assumption has to be backed up by multiple methods, including trustworthy simulations and comparisons to other cluster detections at multiple wavelengths. Using a slightly incorrect selection at low masses could greatly bias the derived constraints. More conservatively, in going to lower masses one needs to consider more general forms for the selection with an increasing number of nuisance parameters (modeling the selection function and mass-richness relation), which would likely degrade cosmological constraints.

It becomes clear nonetheless that if one can properly model the survey completeness and purity down to levels of

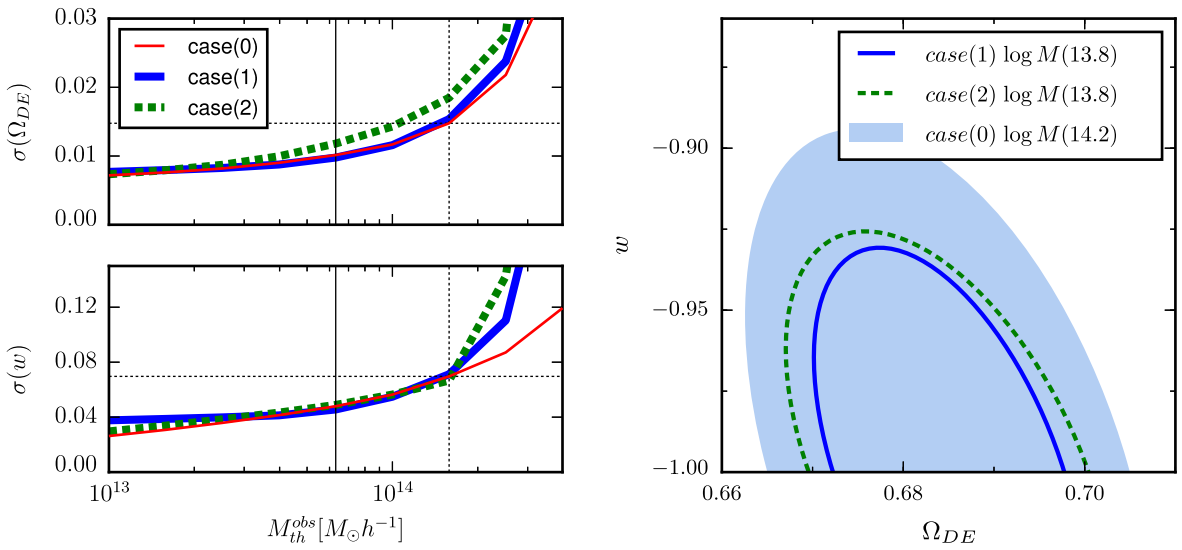


FIG. 4. Left: Constraints on the dark energy parameters $(\Omega_{\rm DE}, w)$ as a function of threshold mass for cases (0), (1), and (2). Even though the constraints are somewhat similar, for case (0) they are only reliable down to $\log[M_{\rm th}^{\rm obs}/(M_\odot h^{-1})] = 14.2$ (dotted vertical line). Right: Constraints for cases (0), (1), and (2) at different threshold masses. The blue shaded region shows constraints for case (0) with its minimum threshold $\log[M_{\rm th}^{\rm obs}/(M_\odot h^{-1})] = 14.2$. Both cases (1) and (2), which include the completeness and purity and go to a lower threshold $\log[M_{\rm th}^{\rm obs}/(M_\odot h^{-1})] = 13.8$, produce better constraints than case (0).

around ∼60%—for which the assumption of perfect selection can no longer be made—the information in cluster counts and clustering is enough to self-calibrate the observable-mass and selection parameters (constrain the parameters along with cosmological parameters), providing better dark energy constraints than fixing conservatively higher thresholds in order to ignore selection effects.

### B. Completeness and purity effects

In this section, for illustrative purposes we focus our discussion on the constraints from case (1), but the results and conclusions for case (2) are similar (see, e.g., Table II). We start by considering baseline constraints for the fiducial model described in Sec. V, assuming perfect knowledge of the observable-mass relation as well as the completeness and purity. In this case the dark energy constraints are $\sigma(\Omega_{\rm DE}, w) = (0.006, 0.033)$. If we let the observable-mass parameters vary freely, but keep the completeness/purity parameters fixed, these constraints degrade to (0.009, 0.044).

Next, we consider the effect of varying the parameters of the completeness and purity. First we fix the observable-mass parameters and let the completeness/purity parameters vary freely. In this case the dark energy constraints become (0.009, 0.042). If we now let both the observable-mass and completeness/purity parameters vary freely, the constraints become (0.010, 0.046). This corresponds to a degradation of (70%, 36%) relative to the case where these functions are perfectly known, but of only (4%, 2%) relative to the case where only the selection is fixed. Therefore, including completeness and purity effects on top of observable-mass parameters avoids biased parameters without significantly degrading the constraints.

Finally, in order to quantify the effects of priors $\sigma_p(\theta_{\rm n})$ assumed on nuisance parameters $\theta_{\rm n} = (\theta_{\rm OM}, \theta_{\rm CP})$, namely, observable-mass parameters $\theta_{\rm OM}$ and/or completeness/purity parameters $\theta_{\rm CP}$, we define the degradation factor $\mathcal{D}_{\theta_{\rm DE}}$ on the constraints of dark energy parameters $\theta_{\rm DE} = (\Omega_{\rm DE}, w)$ as

$$\mathcal{D}_{\theta_{\rm DE}}[\sigma_p(\theta_{\rm n})] = \frac{\sigma[\theta_{\rm DE}|\sigma_p(\theta_{\rm OM}), \sigma_p(\theta_{\rm CP})]}{\sigma(\theta_{\rm DE})|_{\rm ref}} - 1. \quad (26)$$

This factor represents the relative difference between constraints on $\theta_{\rm DE}$ given priors $\sigma_p(\theta_{OM})$ and $\sigma_p(\theta_{CP})$ and the reference ideal case $\sigma(\theta_{\rm DE})|_{\rm ref} = \sigma[\theta_{\rm DE}|0, 0]$ where nuisance parameters are perfectly known.

Applying priors of 1% (or $10^{-2}$ when the fiducial value is zero) on the observable-mass relation parameters but letting the completeness/purity parameters vary freely, the constraints become (0.009, 0.042). Conversely, if we let the observable-mass relation vary freely and apply a 1% prior on the completeness/purity parameters, the constraints become (0.009, 0.044). Finally, by applying a 1% prior to all nuisance parameters (related to the observational effects) the constraints become (0.006, 0.041). This corresponds to a degradation of (8%, 21%) relative to the case in which these nuisance parameters are perfectly known.

External priors may come from multiple sources, including detailed simulations, lensing masses for a subsample of clusters, or cross-matches to clusters detected at other wavelengths, e.g., x-ray and/or millimeter. In all cases, these priors are likely to provide clues to the correct functional forms for these functions and conservative ranges for both the observable-mass relation and the completeness/purity parameters.

Figure 5 shows Fisher constraints—relative to the fiducial value—for each nuisance parameter $\theta_n$. Given that none of these parameters are constrained to better than 10%, having 1% priors on any of these nuisance parameters would have an important effect on constraining the parameters themselves. However, as we have seen the effect on improving dark energy constraints is very small.

Figure 6 shows contours of constant degradation $\mathcal{D}_{\theta_{\rm DE}}$ on the dark energy parameters $\theta_{\rm DE} = (\Omega_{\rm DE}, w)$—relative to perfect nuisance parameters—as a function of priors on the observable-mass relation $\sigma_p(\theta_{\rm OM})$ and on the completeness/purity parameters $\sigma_p(\theta_{\rm CP})$. Notice that both panels of Fig. 6 display similar qualitative behavior, though constraints on $w$ do not degrade as much as constraints on $\Omega_{\rm DE}$. We see that it is important to improve priors on both the observable-mass as well as completeness/purity parameters. For degradations on the dark energy constraints to remain lower than 20%, it is necessary to have quite strong external priors at the subpercent level, which are clearly very hard to achieve even in optimistic scenarios.

TABLE II. Constraints on dark energy parameters $(\Omega_{\rm DE}, w)$ for different priors on the observable-mass parameters $\theta_{\rm OM}$ and the completeness/purity parameters $\theta_{\rm CP}$.

| | | Case (1) | | Case (2) | |
|---|---|---|---|---|---|
| $\theta_{\rm OM}$ | $\theta_{\rm CP}$ | $\sigma(\Omega_{\rm DE})$ | $\sigma(w)$ | $\sigma(\Omega_{\rm DE})$ | $\sigma(w)$ |
| Fix | Fix | 0.006 | 0.033 | 0.006 | 0.036 |
| Free | Fix | 0.009 | 0.044 | 0.010 | 0.047 |
| Fix | Free | 0.009 | 0.042 | 0.010 | 0.045 |
| Free | Free | 0.010 | 0.046 | 0.012 | 0.049 |
| 1% | Free | 0.009 | 0.042 | 0.010 | 0.045 |
| Free | 1% | 0.009 | 0.044 | 0.010 | 0.048 |
| 1% | 1% | 0.006 | 0.041 | 0.007 | 0.042 |

### C. Future surveys

Future surveys [58–60] will allow for improvements in both the total survey area and depth, and the effects of the completeness and purity across these improvements will become more important. The impact of survey depth or maximum redshift $z_{\rm max}$ on dark energy constraints is shown in Fig. 7 and Table III.

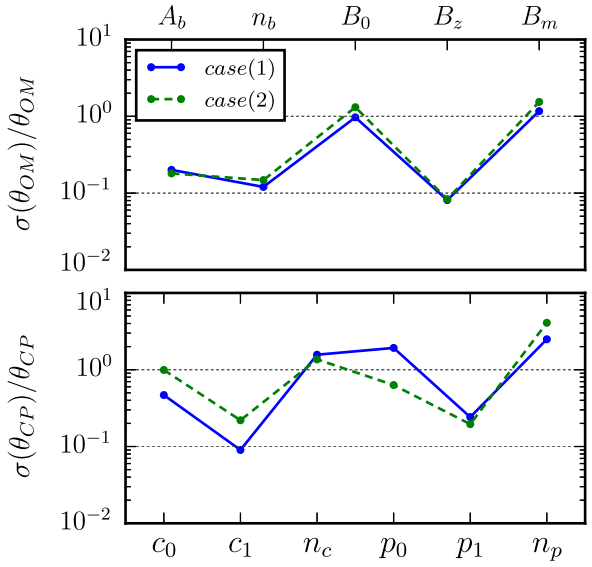


FIG. 5. Fisher constraints derived for nuisance parameters in case (1) (blue solid line) and case (2) (green dashed line). The parameters are related to the observable-mass relation (top panel) and completeness/purity (bottom panel). No priors were assumed for these nuisance parameters.

Optical cluster finders applied to the Sloan Digital Sky Survey (SDSS) in the last decade were limited to relatively shallow magnitudes. For instance, the MaxBCG cluster catalog [24] had $z_{\rm max} = 0.3$, which in our Fisher analysis produces constraints $\sigma(\Omega_{\rm DE}, w) = (0.033, 0.201)$, corresponding to a degradation of (235%, 341%) relative to our fiducial case ($z_{\rm max} = 1.0$). More recently, the redMaPPer cluster finder [26,27] was applied to both the SDSS and the DES Science Verification data, producing catalogs that go up to $z_{\rm max} \sim 0.7$, corresponding to constraints of (0.014, 0.068) and a degradation of (43%, 48%) relative to our fiducial model. Since redMaPPer makes use of the red sequence to detect optical clusters, it may be challenging to extend its results to redshifts much larger than these.

For upcoming surveys planning to extend observations to higher redshifts, we find constraints of (0.008, 0.033) for $z_{\rm max} = 2$, an improvement of (22%, 28%). Case (2) presents a higher degradation when lowering $z_{\rm max}$ than case (1); however, the improvement is lower when we extend $z_{\rm max}$.

We now quantify the impact of the completeness and purity for different values of $z_{\rm max}$ by considering the degradation $\mathcal{D}_{\theta_{\rm DE}}$ on dark energy constraints from Eq. (26), for the case with free completeness and purity parameters $\sigma[\Omega_{\rm DE}|\sigma_p(\theta_{CP}) = \infty]$ relative to the case of perfect knowledge $\sigma[\Omega_{\rm DE}|\sigma_p(\theta_{CP}) = 0]$. In Fig. 8 we see that $\mathcal{D}_{\theta_{\rm DE}}$ has a significant overall improvement (i.e., decrease) with the increase of $z_{\rm max}$ for cases (1) and (2), up to $z_{\rm max} \sim 1.0$–$1.2$. Beyond those redshifts, the degradation increases again, especially for $w$ in case (1). Notice however that these higher degradations are on top of the much improved dark energy constraints (see Table III). Therefore, to fully exploit improvements to cluster dark energy constraints coming from larger survey depths it will be important to properly account for selection effects, despite the fact that it may be significantly harder to quantify these effects at these higher redshifts.

Finally, we quantify the effect of changes in survey area. We keep our approach of considering sample covariance

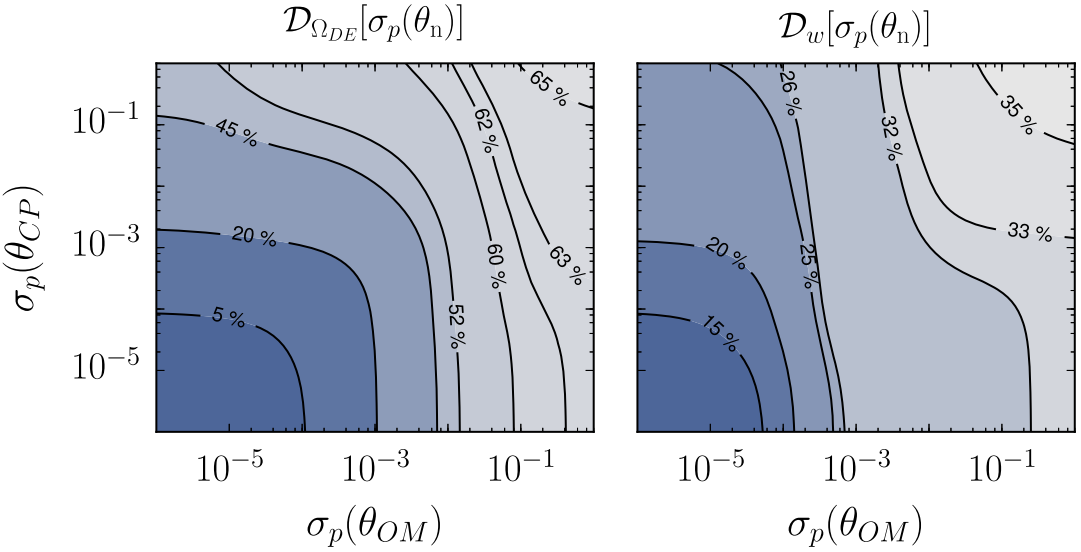


FIG. 6. Contours of constant degradation $\mathcal{D}_{\theta_{\rm DE}}$ on the constraints of dark energy parameters $\theta_{\rm DE} = (\Omega_{\rm DE}, w)$ as a function of priors $\sigma_p(\theta_{\rm OM})$ on all observable-mass relation parameters and priors $\sigma_p(\theta_{\rm CP})$ on all completeness/purity parameters. The degradation is considered for case (1) and relative to the case of perfect nuisance parameters [for which $\sigma_p(\theta_{\rm OM}) = \sigma_p(\theta_{\rm CP}) = 0$]. For $\mathcal{D}_{\theta_{\rm DE}} < 20\%$, subpercent-level priors on all nuisance parameters are required.

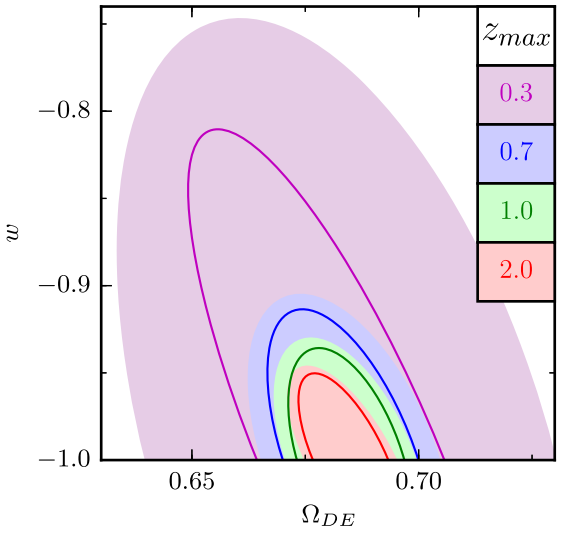


FIG. 7. Effect on dark energy constraints when changing the survey maximum redshift $z_{\rm max}$ from 0.3 (pink), 0.7 (blue), 1.0 (green), and 2.0 (red). Solid lines refer to case (1) and shaded regions refer to case (2).

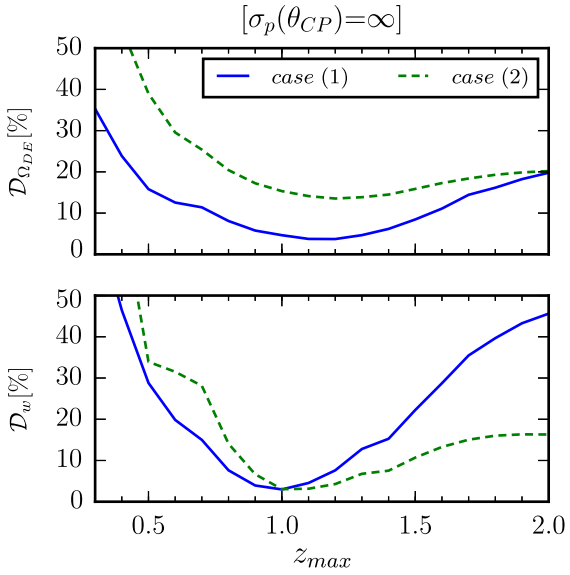


FIG. 8. Percent degradation $\mathcal{D}_{\theta_{\rm DE}}$ on the constraints for dark energy parameters $\theta_{\rm DE} = (\Omega_{\rm DE}, w)$ as a function of maximum redshift $z_{\rm max}$, for the selection function parametrized in case (1) (solid line) and case (2) (dashed line). Degradations are computed for the case where the completeness and purity parameters are free $[\sigma_p(\theta_{\rm CP}) = \infty]$ relative to the case where these parameters are perfectly known $[\sigma_p(\theta_{\rm CP}) = 0]$. $\mathcal{D}_{\theta_{\rm DE}}$ decreases with $z_{\rm max}$ up to $z_{\rm max} \sim 1$ and increases for higher redshifts. The dark energy constraints themselves always improve for higher values of $z_{\rm max}$, but the relative sensitivity to knowledge of the selection parameters increases.

from cells of 10 deg$^2$ and notice that the Fisher matrix has a linear dependence on total area. This means that all constrained parameters have the same degradation/improvements due to changes in the survey area. Our fiducial area of 5000 deg$^2$ is similar to what will be observed by DES. An area twice as large (1/4 of the sky) results in an improvement of ∼29% in both dark energy constraints. For half-sky observations constraints improve by ∼50%, and for full-sky observations they improve by ∼65%.

## VII. DISCUSSION

We have explored the effects of completeness and purity on dark energy constraints from the abundance and clustering of galaxy clusters. We parametrized the selection of cluster samples to reflect a decrease in the completeness and purity at lower masses such that they both reach ∼50% at a mass scale $M \sim 10^{13.5}\ M_\odot/h$. The ratio $(c/p)$ determines the effective selection. Within our parametrization, $(c/p)$ either goes to zero (case 1) or infinity (case 2) as $M \to 0$.

TABLE III. Constraints for dark energy as a function of maximum redshift $z_{\rm max}$. Here all nuisance parameters describing the effective selection function (observable-mass, completeness, and purity) vary freely.

| | Case (1) | | Case (2) | |
|---|---|---|---|---|
| $z_{\rm max}$ | $\sigma(\Omega_{\rm DE})$ | $\sigma(w)$ | $\sigma(\Omega_{\rm DE})$ | $\sigma(w)$ |
| 0.3 | 0.033 | 0.201 | 0.051 | 0.254 |
| 0.5 | 0.018 | 0.089 | 0.025 | 0.100 |
| 0.7 | 0.014 | 0.068 | 0.017 | 0.077 |
| 1.0 | 0.010 | 0.046 | 0.012 | 0.049 |
| 1.2 | 0.009 | 0.040 | 0.010 | 0.044 |
| 1.5 | 0.008 | 0.035 | 0.010 | 0.039 |
| 1.7 | 0.008 | 0.034 | 0.009 | 0.037 |
| 2.0 | 0.008 | 0.033 | 0.009 | 0.035 |

We first considered the bias induced on dark energy constraints when neglecting completeness and purity effects from cases (1) and (2). We found that the bias becomes comparable to dark energy constraints at a threshold mass of $M_{\rm th}^{\rm obs} \sim 10^{14.2}\ M_\odot/h$. As this represents the minimum threshold for which it is safe to ignore selection effects, we then proceeded to study the inclusion of completeness and purity parameters in dark energy constraints for a lower fiducial mass threshold of $M_{\rm th}^{\rm obs} \sim 10^{13.8}\ M_\odot/h$.

Since the effective selection includes not only the completeness and purity but also the observable-mass distribution, the impact of including the completeness and purity depends on the assumptions made for the observable-mass parameters. Within case (1), baseline constraints for fixed observable-mass parameters and fixed completeness and purity are $\sigma(\Omega_{\rm DE}, w) = (0.006, 0.033)$, and when only completeness and purity parameters vary freely these degrade to (0.009, 0.042). On the other hand, if the observable-mass parameters vary freely while

the completeness and purity parameters remain fixed, constraints are $\sigma(\Omega_{\rm DE}, w) = (0.009, 0.044)$ and they only degrade to (0.010, 0.046) if the completeness and purity also vary freely.

Next we considered the impact of external priors on the observable-mass and completeness/purity parameters. From the perspective of dark energy constraints these are nuisance parameters (related to observational effects). We found that joint priors on all nuisance parameters need to be known to better than 1% in order to improve dark energy constraints significantly; with these priors, constraints are restored to $\sigma(\Omega_{\rm DE}, w) = (0.006, 0.041)$ for case (1).

Although it seems unlikely that external priors on selection parameters will reach subpercent levels for current and upcoming cluster surveys, interesting priors should be possible from a combination of multiple sources, including detailed simulations, cross-matches from other surveys, and follow-up spectroscopic observations for a fraction of the cluster sample. For instance, DES has developed detailed simulations that mimic all of its observational properties [61,62]. By running optical cluster finders on these simulations, it is possible to characterize observable-mass and completeness/purity functions [46]. Moreover, DES has a significant overlap with the South Pole Telescope (SPT), so cross-matches of DES optical clusters and SPT Suniaev-Zel'dovich clusters allow for calibrations of the observable-mass relation [38]. A similar calibration can be achieved from x-ray detections [63,64] and lensing masses [65].

Even though our results indicate that only very stringent (and hard to achieve) priors on nuisance parameters would be effective in improving dark energy constraints from self-calibrated constraints (where the nuisance parameters were constrained along the cosmology), such priors are actually very important for checking the validity of the assumed functional forms, thus providing consistency checks for internal self-calibration of nuisance parameters.

We also investigated the effect of changing the survey area (from our fiducial $\Delta\Omega = 5000$ deg$^2$) and maximum redshift (from the fiducial $z_{\rm max} = 1.0$), reflecting expectations from future surveys. For $\Delta\Omega = 10\,000$ deg$^2$ (1/4 of the sky) the constraints would improve by ∼29%, and for $\Delta\Omega = 40\,000$ deg$^2$ (full sky) they would improve by ∼65%, relative to the fiducial case. If we expand the maximum redshift to $z_{\rm max} = 2.0$, constraints on $(\Omega_{\rm DE}, w)$ improve by (22%, 28%) for case (1), though most of this improvement is already achieved for $z_{\rm max} = 1.5$. Despite the improvements to the constraints for higher redshifts and survey areas, these constraints also degrade more significantly due to the lack of knowledge of selection parameters. Therefore, to fully exploit the gain in precision it will be even more important to better understand and calibrate the cluster selection function.

Our results were based on the parametrized functions chosen for the effective selection, and they may depend to some extent on these choices. We proposed functional forms for the completeness and purity, which are inspired by ongoing work involving runs of cluster finders on DES simulations, which we will present elsewhere [46]. In fact, our parametrizations bracket a considerable range of possibilities, so we do not expect significant changes in our conclusions when considering alternative parametrizations. On the other hand, when extending cluster analyses to significantly lower mass thresholds, one needs to ensure that the functional forms are still valid down to those masses, which may be hard even with simulations and multiwavelength cross-matches. In particular, as $c/p$ becomes lower than 50%, we probably need to consider more general functions (or even an arbitrary behavior) for the completeness and purity, which may then significantly degrade dark energy constraints (or even bias them for an oversimplified selection), despite the increase in the number of clusters probed. Again, we envision that detailed simulations and cross-matches should help us in defining the most appropriate parametrizations.

Given that the halo mass function must be known to high precision for cosmological applications [66,67], and the fact that the Tinker mass function is only precise at the 5% level [50], we investigated the effect of changing the halo mass function prescription in our analysis. In real-data analysis one is expected to make use of well-calibrated fitting formulas or emulators for the mass function (see, e.g., Ref. [67]). For illustrative purposes we replaced the Tinker mass function with the fitting formula from Jenkins [68]. We found that this change in the mass function causes variations of up to 20% in the number counts, which leads to changes ≤30% in the cosmological constraints and ≤80% in the constraints of nuisance parameters. However, the degradation effects on the dark energy constraints caused by the inclusion of nuisance parameters remain comparable to those obtained when we use the Tinker mass function (the largest degradation occurs when one of the two sets of nuisance parameters $\theta_{\rm OM}$ or $\theta_{\rm CP}$ is introduced, and the inclusion of the second set is negligible), as does the bias on dark energy parameters introduced by ignoring selection function effects. Therefore, the main conclusions regarding the inclusion/exclusion of nuisance parameters are the same as those presented throughout this work.

Although intrinsic degeneracies always remain to some extent, further improvements in the theoretical modeling of cluster properties coming from $N$-body and gas-dynamics simulations will improve our knowledge of the halo mass function and bias in the presence of baryonic effects [69,70], and help define appropriate functional forms for the observable-mass relation and its intrinsic scatter [31–33]. Improvements in semianalytical halo occupation distribution models will also allow for the creation of reliable mock galaxy catalogs on which we may run cluster finders and calibrate cluster selection parameters. These theoretical developments combined with external calibrations from cluster cross-matches are essential for cluster

cosmology. The self-consistency between observations and theory predictions—which account for all relevant observational effects—will advance our knowledge of the astrophysical processes that regulate observed cluster properties and simultaneously lead to trustworthy cluster cosmological constraints.

## ACKNOWLEDGMENTS

We thank Christophe Benoist, Vinicius Busti, Ricardo Ogando, and Luiz da Costa for useful discussions. M. A. is supported by FAPESP. M. A. and M. L. are partially supported by FAPESP and CNPq.

[1] M. Boylan-Kolchin, V. Springel, S. D. M. White, A. Jenkins, and G. Lemson, Mon. Not. R. Astron. Soc. **398**, 1150 (2009).
[2] A. A. Klypin, S. Trujillo-Gomez, and J. Primack, Astrophys. J. **740**, 102 (2011).
[3] A. Klypin, G. Yepes, S. Gottlöber, F. Prada, and S. Heß, Mon. Not. R. Astron. Soc. **457**, 4340 (2016).
[4] P. Fosalba, M. Crocce, E. Gaztañaga, and F. J. Castander, Mon. Not. R. Astron. Soc. **448**, 2987 (2015).
[5] M. Crocce, F. J. Castander, E. Gaztañaga, P. Fosalba, and J. Carretero, Mon. Not. R. Astron. Soc. **453**, 1513 (2015).
[6] P. Fosalba, E. Gaztañaga, F. J. Castander, and M. Crocce, Mon. Not. R. Astron. Soc. **447**, 1319 (2015).
[7] F. Schmidt, M. Lima, H. Oyaizu, and W. Hu, Phys. Rev. D **79**, 083518 (2009).
[8] M. Lima and W. Hu, Phys. Rev. D **70**, 043504 (2004).
[9] M. Lima and W. Hu, Phys. Rev. D **72**, 043006 (2005).
[10] M. Lima and W. Hu, Phys. Rev. D **76**, 123013 (2007).
[11] H.-Y. Wu, E. Rozo, and R. H. Wechsler, Astrophys. J. **688**, 729 (2008).
[12] B. M. S. Erickson, C. E. Cunha, and A. E. Evrard, Phys. Rev. D **84**, 103506 (2011).
[13] E. Rozo, E. Rykoff, B. Koester, B. Nord, H.-Y. Wu, A. Evrard, and R. Wechsler, Astrophys. J. **740**, 53 (2011).
[14] B. Ascaso *et al.*, Mon. Not. R. Astron. Soc. **456**, 4291 (2016).
[15] B. Ascaso, S. Mei, J. G. Bartlett, and N. Benítez, Mon. Not. R. Astron. Soc. **464**, 2270 (2016).
[16] E. S. Levine, A. E. Schulz, and M. White, Astrophys. J. **577**, 569 (2002).
[17] S. Majumdar and J. J. Mohr, Astrophys. J. **613**, 41 (2004).
[18] M. D. Gladders, H. K. C. Yee, S. Majumdar, L. F. Barrientos, H. Hoekstra, P. B. Hall, and L. Infante, Astrophys. J. **655**, 128 (2007).
[19] C. E. Cunha, Cross-calibration of cluster mass-observables and dark energy, Ph.D. thesis, The University of Chicago, 2008.
[20] C. Cunha, Phys. Rev. D **79**, 063009 (2009).
[21] E. Rozo, R. H. Wechsler, E. S. Rykoff, J. T. Annis, M. R. Becker, A. E. Evrard, J. A. Frieman, S. M. Hansen, J. Hao, D. E. Johnston, B. P. Koester, T. A. McKay, E. S. Sheldon, and D. H. Weinberg, Astrophys. J. **708**, 645 (2010).
[22] B. A. Benson *et al.*, Astrophys. J. **763**, 147 (2013).
[23] P. A. R. Ade *et al.* (Planck Collaboration), Astron. Astrophys. **571**, A20 (2014).
[24] B. P. Koester, T. A. McKay, J. Annis, R. H. Wechsler, A. E. Evrard, E. Rozo, L. Bleem, E. S. Sheldon, and D. Johnston, Astrophys. J. **660**, 221 (2007).
[25] S. Farrens, F. B. Abdalla, E. S. Cypriano, C. Sabiu, and C. Blake, Mon. Not. R. Astron. Soc. **417**, 1402 (2011).
[26] E. S. Rykoff, E. Rozo, M. T. Busha, C. E. Cunha, A. Finoguenov, A. Evrard, J. Hao, B. P. Koester, A. Leauthaud, B. Nord, M. Pierre, R. Reddick, T. Sadibekova, E. S. Sheldon, and R. H. Wechsler, Astrophys. J. **785**, 104 (2014).
[27] E. S. Rykoff *et al.* (DES Collaboration), Astrophys. J. Suppl. Ser. **224**, 1 (2016).
[28] J. P. Dietrich, Y. Zhang, J. Song, C. P. Davis, T. A. McKay, L. Baruah, M. Becker, C. Benoist, M. Busha, L. A. N. da Costa, J. Hao, M. A. G. Maia, C. J. Miller, R. Ogando, A. K. Romer, E. Rozo, E. Rykoff, and R. Wechsler, Mon. Not. R. Astron. Soc. **443**, 1713 (2014).
[29] M. Soares-Santos, R. R. de Carvalho, J. Annis, R. R. Gal, F. La Barbera, P. A. A. Lopes, R. H. Wechsler, M. T. Busha, and B. F. Gerke, Astrophys. J. **727**, 45 (2011).
[30] C. J. Miller, R. C. Nichol, D. Reichart, R. H. Wechsler, A. E. Evrard, J. Annis, T. A. McKay, N. A. Bahcall, M. Bernardi, H. Boehringer, A. J. Connolly, T. Goto, A. Kniazev, D. Lamb, M. Postman, D. P. Schneider, R. K. Sheth, and W. Voges, Astron. J. **130**, 968 (2005).
[31] D. Nagai, Astrophys. J. **650**, 538 (2006).
[32] A. V. Kravtsov, A. Vikhlinin, and D. Nagai, Astrophys. J. **650**, 128 (2006).
[33] D. Nagai, A. Vikhlinin, and A. V. Kravtsov, Astrophys. J. **655**, 98 (2007).
[34] L. Old *et al.*, Mon. Not. R. Astron. Soc. **449**, 1897 (2015).
[35] L. Yu, K. Nelson, and D. Nagai, Astrophys. J. **807**, 12 (2015).
[36] M. Bonamente, M. Joy, S. J. LaRoque, J. E. Carlstrom, D. Nagai, and D. P. Marrone, Astrophys. J. **675**, 106 (2008).
[37] E. S. Rykoff, T. A. McKay, M. R. Becker, A. Evrard, D. E. Johnston, B. P. Koester, E. Rozo, E. S. Sheldon, and R. H. Wechsler, Astrophys. J. **675**, 1106 (2008).
[38] A. Saro *et al.*, Mon. Not. R. Astron. Soc. **454**, 2305 (2015).
[39] M. R. Becker and A. V. Kravtsov, Astrophys. J. **740**, 25 (2011).
[40] D. Gruen, S. Seitz, F. Brimioulle, R. Kosyra, J. Koppenhoefer, C.-H. Lee, R. Bender, A. Riffeser, T. Eichner, T. Weidinger, and M. Bierschenk, Mon. Not. R. Astron. Soc. **442**, 1507 (2014).
[41] A. von der Linden, A. Mantz, S. W. Allen, D. E. Applegate, P. L. Kelly, R. G. Morris, A. Wright, M. T. Allen, P. R. Burchat, D. L. Burke, D. Donovan, and H. Ebeling, Mon. Not. R. Astron. Soc. **443**, 1973 (2014).
[42] A. von der Linden, M. T. Allen, D. E. Applegate, P. L. Kelly, S. W. Allen, H. Ebeling, P. R. Burchat, D. L. Burke,

D. Donovan, R. G. Morris, R. Blandford, T. Erben, and A. Mantz, Mon. Not. R. Astron. Soc. **439**, 2 (2014).
[43] J. P. Dietrich, Y. Zhang, J. Song, C. P. Davis, T. A. McKay, L. Baruah, M. Becker, C. Benoist, M. Busha, L. A. N. da Costa, J. Hao, M. A. G. Maia, C. J. Miller, R. Ogando, A. K. Romer, E. Rozo, E. Rykoff, and R. Wechsler, Mon. Not. R. Astron. Soc. **443**, 1713 (2014).
[44] N. Battaglia *et al.*, J. Cosmol. Astropart. Phys. 08 (2016) 013.
[45] M. Penna-Lima, J. G. Bartlett, E. Rozo, J.-B. Melin, J. Merten, A. E. Evrard, M. Postman, and E. Rykoff, Astron. Astrophys. **604**, A89 (2017).
[46] M. Aguena *et al.* (to be published).
[47] H. Oyaizu, M. Lima, C. E. Cunha, H. Lin, J. Frieman, and E. S. Sheldon, Astrophys. J. **674**, 768 (2008).
[48] F. B. Abdalla, M. Banerji, O. Lahav, and V. Rashkov, Mon. Not. R. Astron. Soc. **417**, 1891 (2011).
[49] C. Sánchez *et al.*, Mon. Not. R. Astron. Soc. **445**, 1482 (2014).
[50] J. Tinker, A. V. Kravtsov, A. Klypin, K. Abazajian, M. Warren, G. Yepes, S. Gottlöber, and D. E. Holz, Astrophys. J. **688**, 709 (2008).
[51] E. J. Baxter, E. Rozo, B. Jain, E. Rykoff, and R. H. Wechsler, Mon. Not. R. Astron. Soc. **463**, 205 (2016).
[52] J. L. Tinker, B. E. Robertson, A. V. Kravtsov, A. Klypin, M. S. Warren, G. Yepes, and S. Gottlöber, Astrophys. J. **724**, 878 (2010).
[53] W. Hu and A. V. Kravtsov, Astrophys. J. **584**, 702 (2003).
[54] W. Hu and A. V. Kravtsov, Astrophys. J. **584**, 702 (2003).
[55] A. Amara and A. Réfrégier, Mon. Not. R. Astron. Soc. **391**, 228 (2008).
[56] P. A. R. Ade *et al.* (Planck Collaboration), Astron. Astrophys. **594**, A13 (2016).
[57] The Dark Energy Survey Collaboration, arXiv:astro-ph/0510346.
[58] eROSITA, http://www.mpe.mpg.de/eROSITA.
[59] Euclid, http://www.euclid-ec.org.
[60] LSST, http://www.lsst.org.
[61] Y. Park *et al.* (DES Collaboration), Phys. Rev. D **94**, 063533 (2016).
[62] E. Suchyta *et al.* (DES Collaboration), Mon. Not. R. Astron. Soc. **457**, 786 (2016).
[63] N. Mehrtens *et al.*, Mon. Not. R. Astron. Soc. **423**, 1024 (2012).
[64] T. Boller, M. J. Freyberg, J. Trümper, F. Haberl, W. Voges, and K. Nandra, Astron. Astrophys. **588**, A103 (2016).
[65] P. Melchior *et al.*, Mon. Not. R. Astron. Soc. **469**, 4899 (2017).
[66] C. E. Cunha and A. E. Evrard, Phys. Rev. D **81**, 083509 (2010).
[67] T. McClintock, E. Rozo, M. R. Becker, J. DeRose, Y.-Y. Mao, S. McLaughlin, J. L. Tinker, R. H. Wechsler, and Z. Zhai, arXiv:1804.05866.
[68] A. Jenkins, C. S. Frenk, S. D. M. White, J. M. Colberg, S. Cole, A. E. Evrard, H. M. P. Couchman, and N. Yoshida, Mon. Not. R. Astron. Soc. **321**, 372 (2001).
[69] W. Cui, S. Borgani, K. Dolag, G. Murante, and L. Tornatore, Mon. Not. R. Astron. Soc. **423**, 2279 (2012).
[70] S. Bocquet, A. Saro, K. Dolag, and J. J. Mohr, Mon. Not. R. Astron. Soc. **456**, 2361 (2016).